

Document downloaded from:

<http://hdl.handle.net/10251/181759>

This paper must be cited as:

Cerqueira, A.; Romero-Gavilán, F.; García-Arnáez, I.; Martínez-Ramos, C.; Ozturan, S.; Izquierdo, R.; Azkargorta, M.... (2021). Characterization of magnesium doped sol-gel biomaterial for bone tissue regeneration: the effect of Mg ion in protein adsorption. *Materials Science and Engineering C: Materials for Biological Applications (Online)*. 125:1-11. <https://doi.org/10.1016/j.msec.2021.112114>



The final publication is available at

<https://doi.org/10.1016/j.msec.2021.112114>

Copyright Elsevier BV

Additional Information

1 **Characterization of magnesium doped sol-gel biomaterial for bone tissue**  
2 **regeneration: the effect of Mg ion in protein adsorption**

3 **Authors**

4 Andreia Cerqueira<sup>1</sup>, Francisco Romero-Gavilán<sup>1\*</sup>, Iñaki García-Arnáez<sup>2</sup>, Cristina Martínez-Ramos<sup>3</sup>, Seda  
5 Ozturan<sup>4</sup>, Raúl Izquierdo<sup>1</sup>, Mikel Azkargorta<sup>5</sup>, Félix Elortza<sup>5</sup>, Mariló Gurruchaga<sup>2</sup>, Julio Suay<sup>1</sup>, Isabel Goñi<sup>2</sup>

6 <sup>1</sup>Department of Industrial Systems Engineering and Design, Universitat Jaume I, Av. Vicent Sos Baynat s/n,  
7 12071 Castellón de la Plana, Spain

8 <sup>2</sup>Departament of Science and Technology of Polymers, Universidad del País Vasco, P. M. de Lardizábal, 3,  
9 20018 San Sebastián, Spain

10 <sup>3</sup>Center for Biomaterials and Tissue Engineering, Universitat Politècnica de Valencia, Camino de Vera, s/n  
11 46022 Valencia, Spain

12 <sup>4</sup>Department of Periodontology, Faculty of Dentistry, Istanbul Medeniyet University, Dumlupınar D100  
13 Karayolu, 98, 34720 Istanbul, Turkey

14 <sup>5</sup>Proteomics Platform, CIC bioGUNE, Basque Research and Technology Alliance (BRTA), CIBERehd, ProteoRed-  
15 ISCIII, Bizkaia Science and Technology Park, 48160 Derio, Spain

16 \*Corresponding author: Francisco Romero-Gavilán

17 Departamento de Ingeniería de Sistemas Industriales y Diseño, Campus del Riu Sec, Avda. Vicent Sos Baynat  
18 s/n, 12071 – Castelló de la Plana (España)

19 E-mail: [gavilan@uji.es](mailto:gavilan@uji.es)

20

21

22

23

24

25

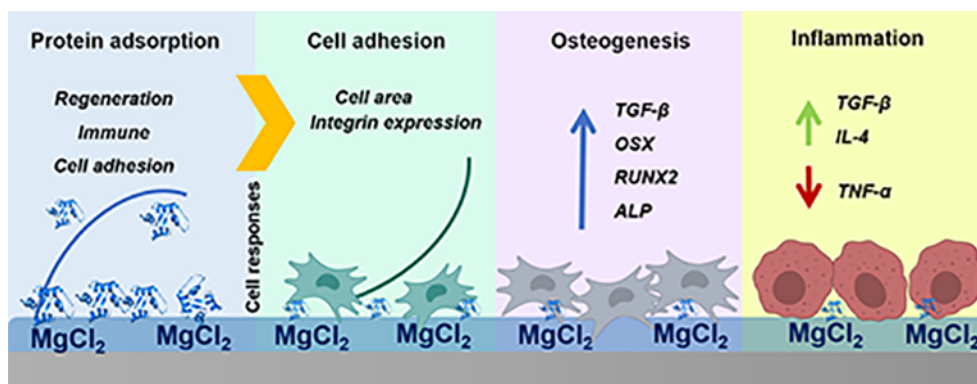
26

27

28 **Abstract**

29 Magnesium is the fourth most abundant element in the human body with a wide battery of functions in the  
30 maintenance of normal cell homeostasis. In the bone, this element incorporates in the hydroxyapatite  
31 structure and it takes part in mineral metabolism and regulates osteoclast functions. In this study, sol-gel  
32 materials with increasing concentrations of MgCl<sub>2</sub> (0.5, 1, and 1.5%) were synthesized and applied onto Ti  
33 surfaces as coatings. The materials were first physicochemically characterized. *In vitro* responses were  
34 examined using the MC3T3-E1 osteoblastic cells and RAW264.7 macrophages. Human serum protein  
35 adsorption was evaluated employing nLC-MS/MS. The incorporation of Mg did not affect the crosslinking of  
36 the sol-gel network, and a controlled release of Mg was observed; it was not cytotoxic at any of the tested  
37 concentrations. The cytoskeleton arrangement of MC3T3-E1 cells cultured on the Mg-doped materials  
38 changed in comparison with controls; the cells became more elongated, with protruded lamellipodia and  
39 increased cell surface. The expression of integrins (ITGA5 and ITGB1) was boosted by Mg-coatings. The ALP  
40 activity and expression of TGF-β, OSX and RUNX2 genes were also increased. In RAW264.7 cells, TNF-α  
41 secretion was reduced, while TGF-β and IL-4 expression rose. These changes correlated with the altered  
42 protein adsorption patterns. The Mg-doped coatings showed increased adsorption of anti-inflammatory  
43 (CLUS, IC1, CFAH, and VTNC), cell adhesion (DSG1, FILA2, and DESP) and tissue regeneration (VTNC and CYTA)  
44 proteins. This integrated approach to biomaterial characterization revealed the potential of Mg in bone tissue  
45 regeneration.

46



47

48 **Keywords**

49 Mg<sup>2+</sup>, biomedical applications, osseointegration, proteomics, hybrids, integrins

50

51

52

## 53 1. Introduction

54 Magnesium (Mg) is the fourth most abundant element in the human body <sup>1</sup>. Approximately 60% of this  
55 element is stored in the bone as a part of the hydroxyapatite structure and takes part in the mineral  
56 metabolism <sup>2,3</sup>. Magnesium is involved in many normal cell functions, such as metabolic reactions and  
57 maintenance of cell membrane, DNA and protein structure. It is a key factor in the translation of genetic  
58 information and adenosine triphosphate (ATP) synthesis <sup>3-5</sup>. Magnesium deficiency has been associated with  
59 the promotion of osteoclastogenesis, which results in decreased bone formation and increased resorption <sup>5</sup>.  
60 Moreover, Mg modulates immune responses by regulating cytokine production <sup>6</sup> and the  
61 activation/suppression of the NF- $\kappa$ B signalling pathway <sup>6,7</sup>. The properties of Mg-based materials have been  
62 attracting increasing attention in the biomedical field. Bioactive glasses <sup>8</sup>, biodegradable alloys (reviewed in  
63 <sup>9</sup>), bioglasses (reviewed in <sup>10</sup>) and Mg-enriched hydroxyapatites <sup>11</sup> have been studied, showing the potential  
64 of new Mg-based materials in bone repair and substitution <sup>12,13</sup>.

65 Titanium (Ti) and its alloys are commonly employed in orthopedic implants used for bone and dental repair  
66 because of their attractive properties such as mechanical strength, excellent resistance to corrosion and  
67 biocompatibility <sup>3</sup>. The successful implementation of these materials depends on the capacity of host bone to  
68 establish intimate contact with the implant surface <sup>14</sup>. However, the relatively bioinert surface of Ti often  
69 causes implant failure and limits its clinical application <sup>3</sup>. Bioactive surface coatings, enhancing the  
70 osteoinductive properties of Ti materials, might present an interesting alternative.

71 The sol-gel technique can be employed to obtain metal surface coatings with a wide variety of advantages,  
72 such as improved control of the chemical composition of the coating and the film microstructure <sup>15</sup>. These  
73 coatings can also be used as controlled release vehicles <sup>16</sup>. Sol-gel precursors are easily available and mix at a  
74 molecular level, allowing the decrease of the sintering temperatures, making it a relatively inexpensive  
75 method <sup>15</sup>. Using 70% of methyltrimethoxysilane (MTMOS) and 30% of tetraethyl orthosilicate (TEOS) as  
76 precursors (MT), Martínez-Ibañez *et al.* <sup>17</sup> have obtained a sol-gel material with biomedical potential. It  
77 showed good osteointegration and osteogenic activity both *in vitro* and *in vivo* <sup>18</sup>. Thus, given the regenerative  
78 potential of magnesium, the development of a sol-gel coating capable of releasing Mg represents an  
79 interesting alternative to bioactivate titanium prostheses.

80 Biological response to an implanted device is determined by the conjugation factors. The initial processes are  
81 crucial. They determine a material outcome *in vivo*, and the provisional matrix formed by blood proteins  
82 adsorbed onto a surface upon implantation defines the consequent cellular and tissular responses <sup>19</sup>. This  
83 protein adsorption depends on the material surface properties, such as wettability, roughness and charge <sup>20</sup>.

84 New sol-gel coatings doped with increasing percentages of Mg (0.5%, 1% and 1.5%) were synthesized to be  
85 applied to a Ti surface. We synthesized the coatings and characterized its physicochemical properties and

86 examined *in vitro* cell responses using the MC3T3-E1 osteoblasts and RAW264.7 macrophages. Human serum  
87 protein adsorption onto the material surface was analyzed employing the nLC-MS. With this results, we aim  
88 to give a broad insight and improve the understanding of the potential of Mg ion in biomedical applications.

## 89 2. Materials and methods

### 90 2.1. Sol-gel synthesis and sample preparation

91 To obtain the hybrid coatings with different percentages of MgCl<sub>2</sub> (**Table 1**), the sol-gel route was employed,  
92 using MTMOS and TEOS precursors in a molar ratio of 7:3. The alkoxy silanes were dissolved in 2-propanol (50  
93 % v/v). The corresponding stoichiometric amount of 0.1N HNO<sub>3</sub> (to hydrolyze the precursors completely), and  
94 the appropriate amounts of MgCl<sub>2</sub> were added to the mix at a rate of 1-drop s<sup>-1</sup>. All the reagents were  
95 purchased from Merck (Darmstadt, Germany). The sol-gel mixtures were kept under stirring for 1 h and then  
96 1 h at rest. Sandblasted, acid-etched (Romero-Gavilán *et al.*<sup>21</sup>) grade-4 Ti discs (12-mm diameter, 1-mm thick)  
97 were used as a substrate for the coatings. The sol-gels were applied with a dip-coater (KSV DC; KSV NIMA,  
98 Espoo, Finland). The discs were immersed in the sol-gel solutions at a speed of 60 cm min<sup>-1</sup>, kept submerged  
99 for one minute, and removed at a 100 cm min<sup>-1</sup>. Glass-slides were employed as a substrate to prepare samples  
100 for hydrolytic degradation and Mg<sup>2+</sup> release assays. The slides were pre-treated with HNO<sub>3</sub> solution (25 % v/v)  
101 in an ultrasonic bath (Sonoplus HD 3200; Bandelin Electronic, Berlin, Germany) for 20 min at 30 W. Next, they  
102 were washed in the ultrasonic bath with distilled water and dried at 100 °C. This pre-treatment aimed to clean  
103 the glass surfaces and ensure the material-glass adhesion. At this point, the glass substrates were coated by  
104 casting. The coating adherence and thickness was measured applying the sol-gel formulations onto AISI 316-  
105 L stainless steel plates (5 cm x 5 cm; RNSinox S.L., Spain). The stainless-steel surfaces were pre-treated by  
106 polishing and cleaned with acetone to remove impurities. The coatings were applied onto the stainless steel  
107 by dip-coating in the same conditions as Ti discs. For thickness measurements, adhesive tape was applied to  
108 the substrate covering a part of it. After dip-coating, the tape was removed creating a border that allows the  
109 thickness measurement of the deposited sol-gel film. For chemical characterization, free films of the  
110 synthesized sol-gel compositions were obtained by pouring the 5 mL of each solution into non-stick Teflon  
111 molds. Finally, to cure the sol-gel, all the samples were subjected to heat treatment, at 80 °C for 2 h.

112 **Table 1.** Nomenclature of the sol-gel networks with different amounts of MgCl<sub>2</sub>. The mass percentages are  
113 relative to the total amount of alkoxy silane.

Nomenclature	Sol-gel network	MgCl <sub>2</sub> (wt%)
MT	70M30T	0
MT0.5Mg	70M30T	0.5
MT1Mg	70M30T	1
MT1.5Mg	70M30T	1.5

114

## 115 **2.2. Physicochemical characterization**

116 A Thermo Nicolet 6700 Fourier-transform infrared spectrometer (FT-IR; Thermo Fisher Scientific, NY, US) with  
117 an attenuated total reflection system (ATR) was employed to characterize the sol-gel networks. The spectra  
118 were measured in the 4000–400  $\text{cm}^{-1}$  wavenumber range. In parallel, the solid-state  $^{29}\text{Si}$  silicon nuclear magnetic  
119 resonance spectroscopy ( $^{29}\text{Si}$ -NMR) technique was used to study the reticulation level of the synthesized  
120 structures. To this purpose, we employed a Bruker 400 AVANCE III WB Plus spectrometer (Bruker, Billerica,  
121 MA, US) with a cross-polarization magic-angle spinning (CP-MAS) probe for solid samples. The pulse sequence  
122 was the Bruker standard: 79.5-MHz frequency, 5-kHz spectral width, 2-ms contact time and 5-s delay time.  
123 The spinning speed was 7.0 kHz. X-ray diffraction analysis (XRD) was carried out to study the crystalline or  
124 amorphous nature of the synthesized materials with a Bruker D4-Endeavor diffractometer (Bruker).  
125 Measurements in the range of 5–70° ( $2\theta$ ) with a step size of 0.02°( $2\theta$ ) and a scanning rate 4 s  $\text{step}^{-1}$  were  
126 collected with filtered  $\text{CuK}\alpha$  radiation ( $\lambda = 1.54 \text{ \AA}$ ), an operating voltage of 40 kV and a filament current of  
127 40 mA. In addition to analyzing the different formulations, with and without magnesium, an  $\text{MgCl}_2$  sample  
128 was analyzed as a control.

129 The coating attachment was analyzed, evaluated and classified by the cross-cut test following the UNE EN-ISO  
130 2409 norm. A mechanical profilometer Dektack 6 (Veeco; Munich, Germany) was employed to measure the  
131 thickness of the coating applied onto the stainless steel plates. Profiles from the uncoated area to the coated  
132 area were taken, measuring the rise between coated and uncoated areas. Three individual samples were  
133 analyzed, performing three measurements in each of them.

134 A scanning electron microscope (SEM; Leica-Zeiss LEO, Leica, Wetzlar, Germany) was used to examine the  
135 coating morphologies onto Ti discs. Platinum sputtering was employed to increase the sample conductivity.  
136 An optical profilometer PLm2300 (Sensofar, Barcelona, Spain) was used to characterize the sample roughness.  
137 Three samples of each material were evaluated, and three measurements were carried out for each sample  
138 to obtain an average value of  $R_a$  (arithmetic average roughness parameter) for each surface. An automatic  
139 contact angle meter OCA 20 (DataPhysics Instruments, Filderstadt, Germany) was employed to characterize  
140 the surface wettability of the coated Ti surfaces. Ultrapure water drops of 10  $\mu\text{L}$  were deposited on the  
141 material at a speed of 27.5  $\mu\text{L s}^{-1}$ . The drop images were examined using SCA 20 software (DataPhysics  
142 Instruments). Six samples of each type were tested, depositing two drops on each disc.

143 The mass loss during sample incubation in 50 mL of distilled water at 37 °C was recorded to examine the rate  
144 of hydrolytic degradation. Samples were removed after 7, 14, 28, 42, and 56 days of incubation. The results  
145 were calculated as a percentage (%) of the initial mass lost. Three independent samples were evaluated for  
146 each condition. The amount of  $\text{Mg}^{2+}$  released from the coatings was measured using an inductively coupled

147 plasma mass spectrometer (Agilent 7700 Series ICPMS; Agilent Technologies, Santa Clara, CA, US). The  
148 materials were incubated in ddH<sub>2</sub>O at 37 °C for 28 days. Aliquots of 0.5 mL were removed after 2, 4, 6, 8, 24,  
149 72, 168, 336, 504 and 672 h of incubation. Each data point is the average of the values obtained for three  
150 replicas.

## 151 **2.3. In vitro assays**

### 152 **2.3.1. Cell culture**

153 Mouse calvaria osteosarcoma (MC3T3-E1) cell line was seeded onto the materials in low-glucose DMEM  
154 (Gibco, Life Technologies, Thermo Fisher Scientific) with 1 % penicillin/streptomycin (Gibco) and 10 % foetal  
155 bovine serum (FBS; Gibco). After 24 h, the cell culture medium was replaced with osteogenic medium (DMEM,  
156 1 % penicillin/streptomycin, 10 % FBS, 1 % ascorbic acid (5 µg mL<sup>-1</sup>), and 100 mM β-glycerol phosphate), which  
157 was changed every two days. Mouse murine macrophage (RAW264.7) cell line was cultured in high-glucose  
158 DMEM supplemented with 1 % penicillin/streptomycin and 10 % FBS. Cell culture was carried out in a  
159 humidified (95 %) incubator at 37 °C, with 5 % CO<sub>2</sub>.

### 160 **2.3.2. Cytoskeleton arrangement**

161 For the evaluation of cytoskeleton arrangement, MC3T3-E1 cells were seeded on the materials at a density of  
162 1 x 10<sup>4</sup> cells cm<sup>-2</sup> for 1 day. Then, the samples were washed once with PBS, fixed with 4 % paraformaldehyde  
163 (PFA) for 20 min at room temperature and permeabilized with 0.1 % Triton X-100 for 5 min. Next, the samples  
164 were incubated with phalloidin (1:100; Abcam, Cambridge, UK) diluted in 0.1 % w/v bovine serum albumin  
165 (BSA)-PBS for 1 h at room temperature. For nuclei staining, after washing twice with PBS, the samples were  
166 incubated for 5 min in a mounting medium with DAPI (Abcam). A Leica TCS SP8 Confocal Laser Scanning  
167 Microscope with 20x (dry) lenses was employed for fluorescence detection. The images were obtained using  
168 LAS X software (Leica) and analyzed using Image J software (National Institutes of Health, Maryland, USA).

### 169 **2.3.3. Cytotoxicity and ALP activity**

170 Biomaterial cytotoxicity was assessed using the MC3T3-E1 cells, following the ISO 10993-5:2009 (Annex C) <sup>22</sup>  
171 standards, and samples were prepared according to the ISO 10993-12:2012 <sup>23</sup>. The CellTiter 96® Proliferation  
172 Assay (MTS; Promega, Madison, WI), based on the formazan formation, was used according to manufacturer's  
173 guidelines. For controls, cells incubated without (negative control) and with latex (positive control) were used.  
174 The material was considered cytotoxic when the cell viability fell below 70 %.

175 To evaluate the effects on cell mineralization, the MC3T3-E1 cells were cultured on the materials at a density  
176 of 1.75 x 10<sup>4</sup> cells cm<sup>-2</sup> for 7 and 14 days. At each time point, alkaline phosphatase activity (ALP) activity was

177 measured following the protocol of Araújo-Gomes *et al.*<sup>18</sup> and normalized to protein content obtained using  
178 a Pierce BCA assay kit (Thermo Fisher Scientific).

#### 179 **2.3.4. Cytokine quantification using ELISA**

180 For measuring the levels of secreted cytokines, the cell culture medium used to incubate the RAW264.7 cell-  
181 seeded discs was collected and frozen until further analysis. The concentrations of tumor necrosis factor  
182 (TNF)- $\alpha$  and transforming growth factor (TGF)- $\beta$  were determined using an ELISA (Invitrogen, Thermo Fisher  
183 Scientific) kit, according to the manufacturer's instructions.

#### 184 **2.3.5. Relative gene expression: RNA extraction, cDNA synthesis and qRT-PCR**

185 To examine the effects of the Mg-doped materials on gene expression, the MC3T3-E1 cell line was cultured at  
186 a density of  $1.75 \times 10^4$  cells  $\text{cm}^{-2}$  for 7 and 14 days and RAW264.7 at a density of  $30 \times 10^4$  cells  $\text{cm}^{-2}$  for 2 and  
187 4 days. Total RNA was extracted with TRIzol as described in Cerqueira *et al.*<sup>24</sup>. RNA concentration, integrity,  
188 and quality were measured using NanoVue<sup>®</sup> Plus Spectrophotometer (GE Healthcare Life Sciences, Little  
189 Chalfont, UK). For cDNA synthesis, approximately 1  $\mu\text{g}$  of total RNA was converted into cDNA using PrimeScript  
190 RT Reagent Kit (Perfect Real Time; TAKARA Bio Inc., Shiga, Japan). The reaction was carried out in a Prime  
191 Thermal Cycler (Techne, Staffordshire, UK) as described in Cerqueira *et al.*<sup>24</sup>. The resulting cDNA was diluted  
192 in DNase-free water to a concentration suitable for gene expression evaluation.

193 Quantitative real-time PCRs (qRT-PCR) were carried out in 96-well plates (Applied Biosystems<sup>®</sup>, Thermo Fisher  
194 Scientific). Each sample represented the gene of interest and the housekeeping gene (*GAPDH*). Primers for  
195 each gene were designed (using Primer3Plus software tool) from specific DNA sequences obtained from NCBI  
196 and purchased from Thermo Fisher Scientific. The targets studied for each cell line are shown in  
197 **Supplementary Table 1**. Reactions were carried out as described in Cerqueira *et al.*<sup>24</sup> in a StepOne Plus<sup>™</sup> Real-  
198 Time PCR System (Applied Biosystems<sup>®</sup>). Fold changes were calculated using the  $2^{-\Delta\Delta\text{Ct}}$  method, and data were  
199 normalized to blank wells (without materials).

#### 200 **2.4. Adsorbed protein layer and proteomic analysis**

201 To obtain the proteins adsorbed onto the material surface, samples were incubated for 3 h (37 °C, 5 % CO<sub>2</sub>) in  
202 24-well NUNC plates (Thermo Fisher Scientific) with 1 mL of human serum from male AB plasma (Merck). The  
203 materials were washed five times with ddH<sub>2</sub>O and once with wash buffer (100 mM NaCl, 50 mM Tris-HCl, pH  
204 7.0) to eliminate non-adsorbed proteins. Adsorbed proteins were obtained by elution (0.5 M  
205 triethylammonium bicarbonate buffer (TEAB), 4 % sodium dodecyl sulfate (SDS), 100 mM dithiothreitol (DTT);  
206 Merck). For each surface, four independent replicates were analyzed, and each replicate was a pool of eluate  
207 from four discs. Total serum protein concentration was determined using a Pierce BCA assay kit (Thermo  
208 Fisher Scientific).



209 For proteomic analysis, the eluate was characterized employing electrospray tandem mass spectrometry,  
210 using a nanoACQUITY UPLC (Waters, Milford, MA) coupled to an Orbitrap XL (Thermo Electron, Bremen,  
211 Germany), following the protocol described in Romero-Gavilán *et al.* <sup>25</sup>. Each sample was analyzed in  
212 quadruplicate. Proteomic results were examined using PEAKS (Bioinformatics Solutions Inc., Waterloo,  
213 Canada), and the functional classification of the identified proteins was performed employing PANTHER  
214 software (<http://www.pantherdb.org/>).

## 215 **2.5. Statistical analysis**

216 Physicochemical and *in vitro* assay data were analyzed via one-way analysis of variance (ANOVA) with Tukey  
217 post hoc test, after confirming normal distribution and equal variance. Statistical analysis was performed using  
218 GraphPad Prism 5.04 software (GraphPad Software Inc., La Jolla, CA). The differences between MT and Mg-  
219 doped MT were considered statistically significant at  $p \leq 0.05$  (\*),  $p \leq 0.01$  (\*\*), and  $p \leq 0.001$  (\*\*\*). Data were  
220 expressed as means  $\pm$  standard error (SE).

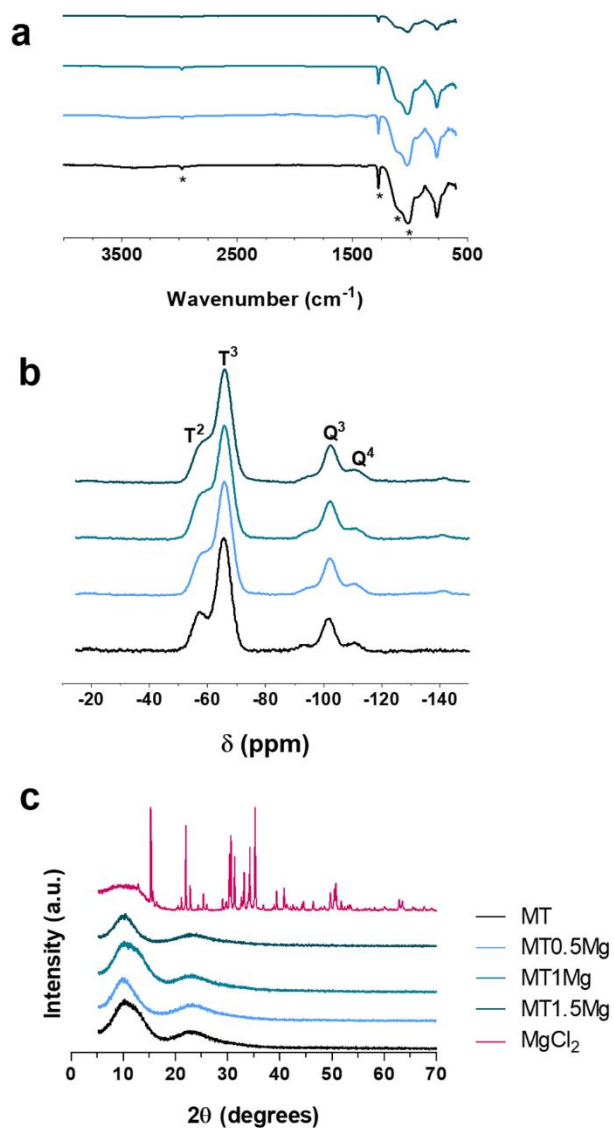
221 In the proteomic analysis, a Student's *t*-test was conducted to evaluate differences between MT and MT with  
222 different Mg concentrations, using Progenesis software. Differences were considered statistically significant  
223 at  $p \leq 0.05$  and the ratio difference bigger than 1.3 in either direction (higher or lower).

## 224 **3. Results**

### 225 **3.1. Physicochemical characterization**

226 Hybrid sol-gel networks containing different amounts of MgCl<sub>2</sub> were synthesized using the sol-gel route. The  
227 effect of this compound on the sol-gel structure was studied using FT-IR, <sup>29</sup>Si-NMR and XRD (**Figure 1**). The FT-  
228 IR spectra demonstrated the presence of MTMOS-associated organic groups in the final networks; the bands  
229 corresponding to Si-C and C-H bonds were detected at 1270 and 2980 cm<sup>-1</sup> <sup>26</sup>, respectively. The signals seen  
230 at 760, 1020 and 1120 cm<sup>-1</sup> were related to the formation of Si-O-Si bonds, and the band at 950 cm<sup>-1</sup> indicated  
231 the presence of non-condensed Si-OH species <sup>21</sup>. These results are confirmed by the <sup>29</sup>Si-NMR spectra, which  
232 can verify the proper formation of the polysiloxane network (**Figure 1b**). Signals associated with the MTMOS  
233 trifunctional alkoxy silane (T units) are detected between -50 and -70 ppm. Within this range, the peaks at -57  
234 and -66 ppm indicate the presence of T<sup>2</sup> and T<sup>3</sup> species <sup>26</sup>, respectively. The TEOS tetrafunctional (Q units)  
235 chemical shifts are in the range between -97.5 and -115 ppm; the signals at -102 and -110 ppm reflect the  
236 presence of Q<sup>3</sup> and Q<sup>4</sup> species, respectively <sup>27</sup>. A good degree of crosslinking was achieved in the materials  
237 synthesized here; only the species with the highest degree of condensation were detected in the sol-gel  
238 structure. Moreover, it seems that the MgCl<sub>2</sub> incorporation into the sol-gel did not affect the final silica  
239 network crosslinking as all the spectrum shapes were similar. **Figure 1c** shows the XRD spectra obtained for  
240 the different sol-gel materials and for the MgCl<sub>2</sub>. The obtained patterns for all the sol-gel formulations doped  
241 with MgCl<sub>2</sub> can be associated with an amorphous nature as no peaks related to MgCl<sub>2</sub> or other crystalline

242 structures were detected. In addition, no significant differences were found between the distinct Mg-doped  
243 compositions and MT. The broad and undefined peak around  $10^\circ$  ( $2\theta$ ) in the sol-gel material spectra can be  
244 associated with the presence of not completely hydrolyzed precursors. Another peak with similar shaped but  
245 less intensity was detected around  $21^\circ$  ( $2\theta$ ), being this signal characteristic of the  $\text{SiO}_2$  amorphous sol-gel  
246 structures<sup>28</sup>.



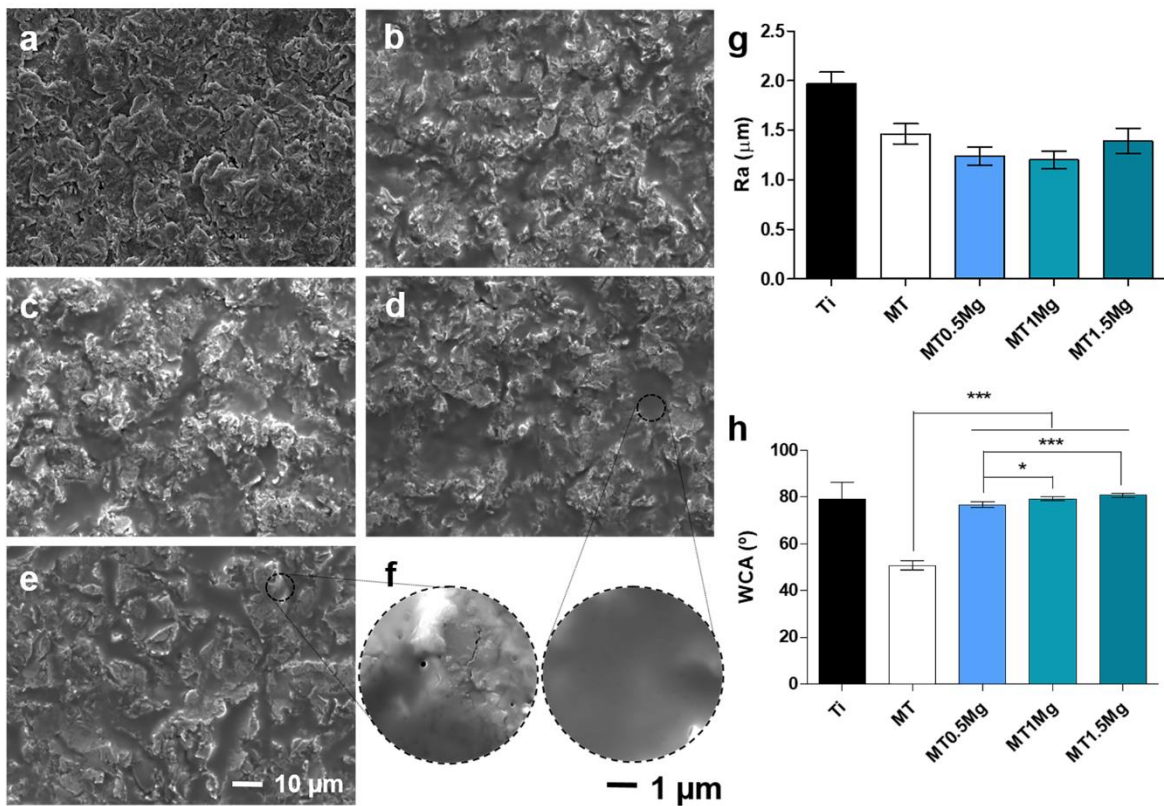
247

248 **Figure 1:** (a) FT-IR, (b)  $^{29}\text{Si}$ -NMR and (c) XRD spectra of the studied sol-gel networks.

249

250 All sol-gel materials coatings showed a high degree of adherence (Class 0) based on the cross-cut test, as the  
251 edges of the cuts were smooth, and detachments were not observed (**Supplementary Figure 1a**). The coatings  
252 applied onto Ti were morphologically evaluated by SEM. The micrographs show that the different

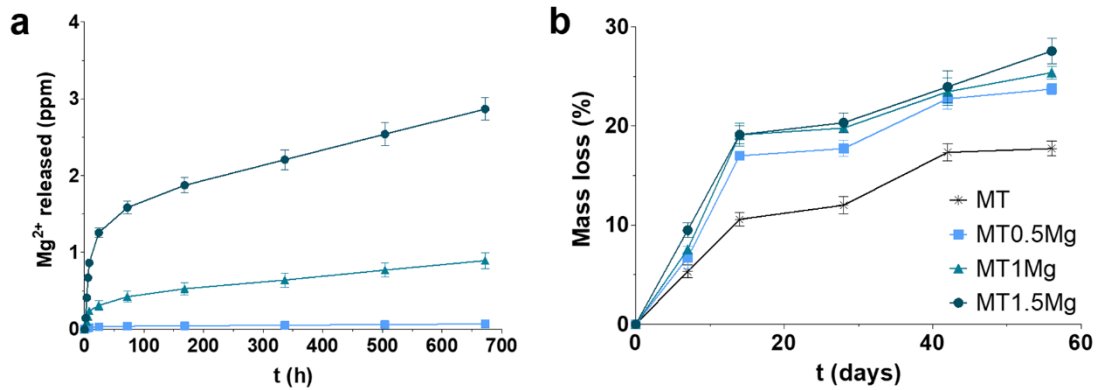
253 compositions covered the whole area of Ti substrates (**Figure 2a-e**). Nevertheless, the sol-gel seemed to  
 254 accumulate in the cavities associated with the Ti roughness, smoothing the initial morphological irregularities  
 255 of the Ti surface. No MgCl<sub>2</sub> precipitates were detected. However, small holes of around 0.2–0.3 μm in diameter  
 256 can be seen in the film with the largest amount of MgCl<sub>2</sub> (MT1.5Mg); these are not observed in other  
 257 compositions (**Figure 2f**). The materials with MgCl<sub>2</sub> have the Ra roughness values similar to the Ra of the  
 258 coating without Mg salt (**Figure 2g**). Additionally, the thickness measurements for the different coatings  
 259 showed that the obtained sol-gel films do not have differences in thickness regardless of the amount of MgCl<sub>2</sub>  
 260 added (**Supplementary Figure 1b**). The wettability results showed higher contact angles for materials with Mg  
 261 than for the MT base material (**Figure 2h**). The coatings with MgCl<sub>2</sub> were more hydrophobic than MT, reaching  
 262 the values of around 80° (close to those for uncoated Ti).



263  
 264 **Figure 2:** SEM microphotographs of (a) Ti, (b) MT, (c) MT0.5Mg, (d) MT1Mg, (e) MT1.5Mg and (f) enlarged  
 265 areas of MT1Mg and MT1.5Mg coatings. Scale bars: (a-e) 10 and (f) 1 μm. Roughness Ra (g) and contact angle  
 266 (WCA; h) are also displayed. Results are shown as means ± SE. The asterisks ( $p \leq 0.05$  (\*) and  $p \leq 0.001$  (\*\*\*))  
 267 indicate significant differences between MT and Mg-doped MT.

268 The Mg-containing coatings had a higher degradation rate than the base coating MT (**Figure 3a**). The base  
 269 network showed a mass loss of around 18 % after 56 days of incubation. This mass loss increased as more  
 270 MgCl<sub>2</sub> was incorporated into the sol-gel, reaching a value of around 28 % for the MT1.5Mg coating. The

271 amount of  $Mg^{2+}$  ions released also rose with the increasing salt content in the sol-gel compositions (**Figure**  
272 **3b**). Moreover, the  $Mg^{2+}$  liberation process continued throughout the studied period (28 days).



273

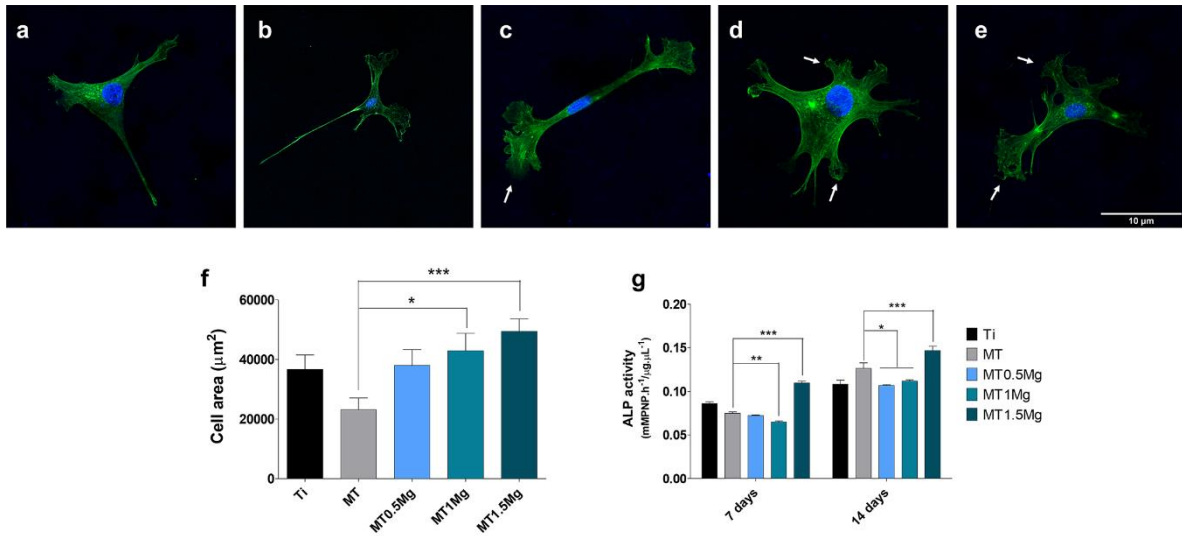
274 **Figure 3:** Release kinetics of  $Mg^{2+}$  ions (a) and hydrolytic degradation (b) of the sol-gel coatings enriched with  
275  $MgCl_2$ . Bars indicate standard errors.

## 276 3.2. In vitro assays

### 277 3.1.1. Cytoskeleton arrangement, cytotoxicity and ALP activity

278 To examine the arrangement of cellular cytoskeleton, the cells were stained with phalloidin after 1 day of  
279 culture (**Figure 4 a-e**). The cells cultured on Ti and MT showed a triangular shape with few lamellipodia, while  
280 cells on the materials with Mg displayed a more elongated with protruding lamellipodia (white arrows). The  
281 MC3T3-E1 cells cultured on MT1Mg and MT1.5Mg also displayed protruding filopodia. Cells growing on  
282 MT1Mg and MT1.5Mg materials had significantly larger surface area than those cultured on the MT discs  
283 (**Figure 4f**).

284 None of the materials in the study was cytotoxic (data not shown). ALP activity showed a small decrease for  
285 MT0.5Mg and MT1Mg at 7 and 14 days, and a significant activity increase at 7 and 14 days for MT1.5Mg  
286 (**Figure 4g**).

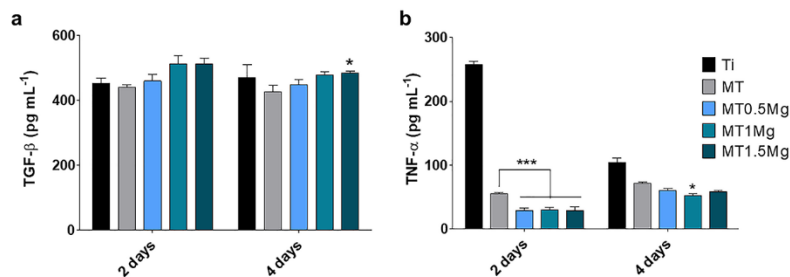


287

288 **Figure 4:** Fluorescent confocal images of cytoskeleton arrangement of MC3T3-E1 on (a) Ti, (b) MT, (c)  
 289 MT0.5Mg, (d) MT1Mg and (e) MT1.5Mg and (f) area of the cells adhered to the materials (f). Actin filaments  
 290 were stained with phalloidin (green), and nuclei were stained with DAPI (blue). Scale bar: 10 μm. ALP activity  
 291 (g) of MC3T3-E1 cells at 7 and 14 days. Results are shown as means ± SE. The asterisks ( $p \leq 0.05$  (\*),  $p \leq 0.01$   
 292 (\*\*), and  $p \leq 0.001$  (\*\*\*)) indicate statistically significant differences between MT and Mg-doped MT.

### 293 3.1.2. Cytokine secretion measurements by ELISA

294 To evaluate the effect of Mg-doped materials on inflammation, cytokine secretion to the RAW264.7 cell  
 295 culture medium was examined. The levels of anti-inflammatory cytokine TGF-β increased significantly only in  
 296 cultures on MT1.5Mg, at 4 days (**Figure 5a**). In contrast, after 2 days, the amounts of secreted pro-  
 297 inflammatory cytokine TNF-α significantly decreased for all materials (**Figure 5b**). After 4 days, the TNF-α  
 298 excretion levels were similar for all the materials, with a significant decrease for MT1Mg in comparison with  
 299 MT.

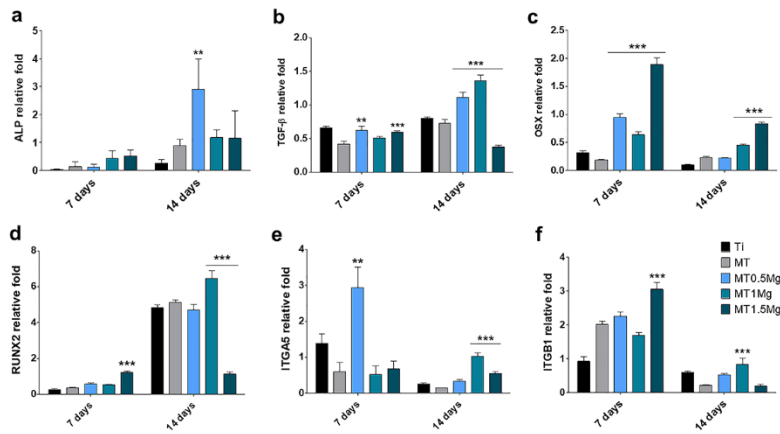


300

301 **Figure 5:** ELISA results for (a) TGF-β and (b) TNF-α for RAW264.7 cultures at 2 and 4 days. Data are shown as  
 302 means ± SE. The asterisks ( $p \leq 0.05$  (\*),  $p \leq 0.001$  (\*\*\*)) indicate statistically significant differences between  
 303 MT and Mg-doped MT.

304 **3.1.3. Relative gene expression**

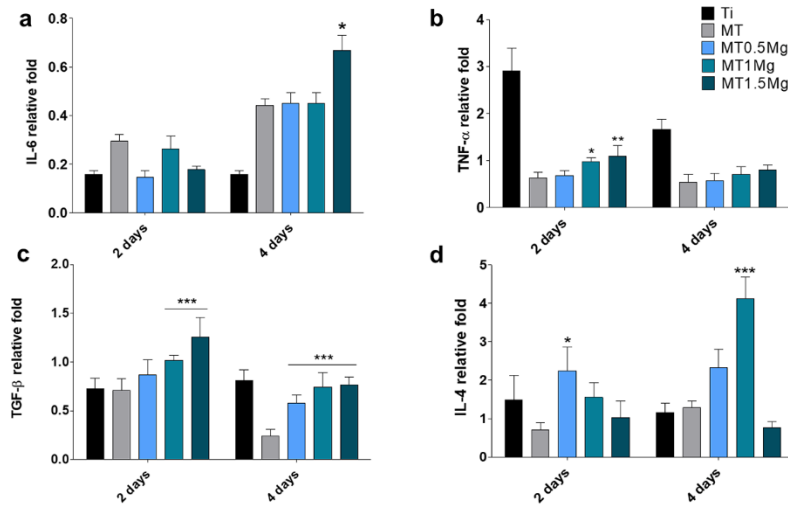
305 To further understand the effects of the Mg-doped materials on osteogenesis (ALP, TGF- $\beta$ , OSX, and RUNX2),  
 306 cell adhesion (ITGA5 and ITGB1), and inflammatory responses (IL-6, TNF- $\alpha$ , TGF- $\beta$ , and IL-4), gene expression  
 307 of selected targets was measured. In the case of osteogenic markers, after 7 days of culture, the ALP  
 308 expression was similar for all materials. However, there was a significant increase in its expression on  
 309 MT0.5Mg at 14 days (**Figure 6a**). The TGF- $\beta$  expression was increased in MT0.5Mg and MT1.5Mg after 7 days.  
 310 After 14 days, it was significantly augmented in MT0.5Mg and MT1Mg cultures and decreased on MT1.5Mg  
 311 materials (**Figure 6b**). The expression of OSX showed a significant increase for all Mg-doped materials at both  
 312 time points (**Figure 6c**). The expression of RUNX2 was only augmented for MT1.5Mg at 7 days. After 14 days,  
 313 it increased significantly in the MT1Mg cultures and decreased for MT1.5Mg (**Figure 6d**). In the case of cell  
 314 adhesion markers, ITGA5 expression rose for MT0.5Mg at 7 days and for MT1Mg and MT1.5Mg at 14 days  
 315 (**Figure 6e**). The expression of ITGB1 increased for MT1.5Mg at 7 days, and for MT1Mg at 14 days (**Figure 6f**).



316

317 **Figure 6:** Gene expression of (a) alkaline phosphatase (ALP), (b) transforming growth factor (TGF- $\beta$ ), (c) osterix  
 318 (OSX), (d) runt-related transcription factor 2 (RUNX2), (e)  $\alpha$ 5-integrin (ITGA5), and (f)  $\beta$ 1-integrin (ITGB1) in  
 319 MC3T3-E1 cultures at 7 and 14 days. Gene expression was normalized to blank wells (without any material)  
 320 using the  $2^{-\Delta\Delta Ct}$  method. Results are shown as means  $\pm$  SE. The asterisks ( $p \leq 0.05$  (\*),  $p \leq 0.01$  (\*\*), and  $p \leq$   
 321 0.001 (\*\*\*)) indicate statistically significant differences between MT and Mg-doped MT.

322 Among the genes related to macrophages responses, the expression of pro-inflammatory marker IL-6 was  
 323 significantly altered only in MT1.5Mg cultures at 4 days (**Figure 7a**), while TNF- $\alpha$  expression increased for  
 324 MT1Mg and MT1.5Mg at 2 days (**Figure 7b**). The expression of anti-inflammatory marker TGF- $\beta$  (**Figure 7c**)  
 325 increased on MT1Mg and MT1.5Mg at 2 days. All the materials showed an increase in its expression at 4 days.  
 326 The expression of IL-4 was rose for MT0.5Mg at 2 days and for MT1Mg, at 4 days (**Figure 7d**).



327

328 **Figure 7:** Gene expression of (a) interleukin (IL)-6, (b) tumor necrosis factor (TNF)- $\alpha$ , (c) transforming growth  
 329 factor (TGF)- $\beta$ , and (d) IL-4 in RAW264.7 macrophages after 2 and 4 days of culture. Gene expression was  
 330 normalized to blank wells (without any material) using the  $2^{-\Delta\Delta Ct}$  method. Results are shown as means  $\pm$  SE.  
 331 The asterisks ( $p \leq 0.05$  (\*),  $p \leq 0.01$  (\*\*), and  $p \leq 0.001$  (\*\*\*)) indicate statistically significant differences  
 332 between MT and Mg-doped MT.

### 333 3.3. Proteomic analysis

334 The nLC-MS/MS analysis of eluted proteins identified 22 proteins preferentially adsorbed on the materials  
 335 with Mg in comparison with the MT base material (**Supplementary Table 2; Table 2**). Among these, six  
 336 proteins are related to complement system activation (CO9, CO3 and C1QC) and its inhibition (IC1, CLUS, and  
 337 CFAH). Some other proteins associated with immune responses were also more abundant on the Mg-doped  
 338 coatings. A1AT, which regulates the activity of neutrophil granulocytes, two immunoglobulins (LAC3 and  
 339 IGHM) and a pentraxin (SAMP) were more absorbed. Three cell adhesion proteins preferentially attached to  
 340 the materials containing Mg (DSG1, FILA2 and DESP). Similarly, VTNC and CYTA, which present a battery of  
 341 functions related to tissue regeneration, regulation/inhibition of immune responses and cell attachment,  
 342 preferentially adhered to Mg-doped MT. Moreover, several apolipoproteins related to lipid metabolism  
 343 (APO2, APOA1, APOA4 and APOL1) were identified as well as two proteins associated with coagulation (SPB12  
 344 and A2MG) and one associated with DNA damage repair (UBB).

345 PANTHER analysis was used to associate the differentially adsorbed proteins with their biological functions  
 346 and pathways. **Figure 6** shows pie-chart diagrams of the biological functions and pathways for the proteins  
 347 differentially adsorbed onto the Mg-doped surfaces in comparison with MT. Among the various biological  
 348 functions found, the immune system, cellular organization and process, multi-organism and multicellular  
 349 organismal process, biological regulation, developmental and metabolic process and biological adhesion were

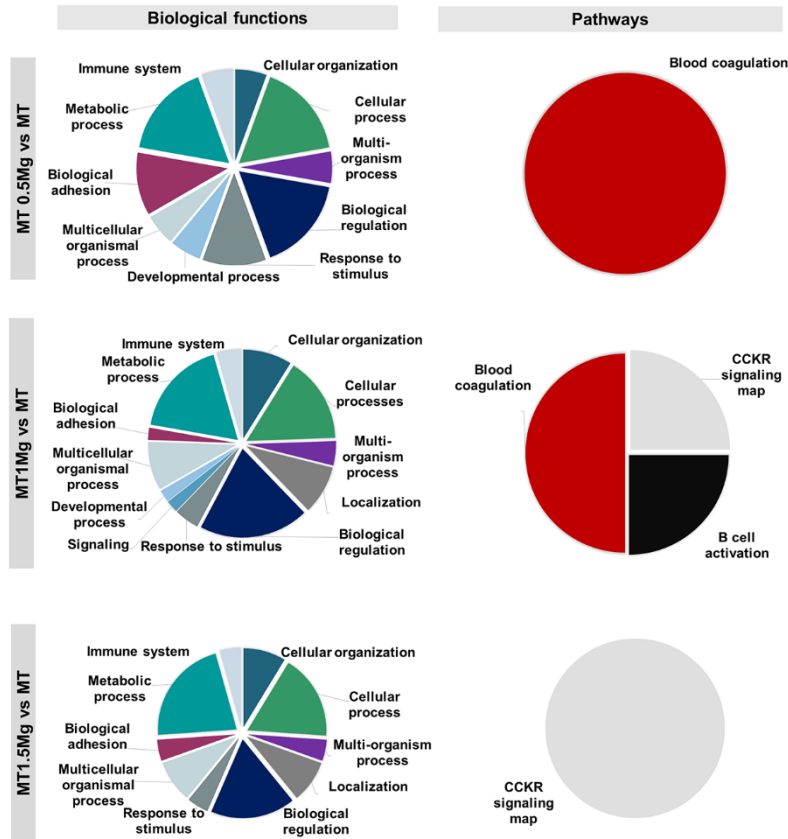
350 identified for all materials with Mg. For MT1Mg and MT1.5Mg, signaling and biological functions also  
 351 appeared. The search for pathway associations revealed blood coagulation pathway for proteins from  
 352 MT0.5Mg and MT1Mg materials. For the MT1Mg material, CCKR signaling map and B cell activation were also  
 353 identified. For MT1.5Mg, only the CCKR signaling map pathway appeared.

354 **Table 2.** Ratios of different proteins differentially adsorbed onto the sol-gel materials doped with Mg,  
 355 associated with relevant biological processes (immune response, cell adhesion, tissue regeneration and  
 356 coagulation).

Protein	Biological process	Ratio		
		MT0.5Mg/MT	MT1Mg/MT	MT1.5Mg/MT
CO9		2.13	16.17	11.05
SAMP		6.97	12.77	9.63
CLUS		6.20	8.07	7.36
CFAH		3.63	5.51	5.34
A1AT		4.04	3.96	4.16
LAC3		1.00	6.54	3.69
IC1	Immune responses	2.91	3.47	3.56
C1QC		2.25	3.14	3.31
CO3		1.51	1.79	1.86
IGHM		1.37	2.17	1.84
APOA2		1.66	17.26	10.16
APOA1		1.18	2.73	3.52
APOA4		1.68	3.97	2.42
APOL1		1.18	4.50	2.32
CYTA	Tissue regeneration	2.24	10.68	10.89
VTNC		2.07	3.28	3.86
DSG1	Cell adhesion	11.36	19.75	10.57
FILA2		3.18	39.49	5.21
DESP		6.07	3.78	1.90
SPB12	Coagulation	1.50	6.05	4.00
A2MG		5.29	5.11	2.13

357





358

359 **Figure 8:** PANTHER diagram of biological functions and pathways associated with the proteins differentially  
 360 adhering to Mg-enriched coatings in comparison with MT (without Mg).

361 **4. Discussion**

362 For a successful bone substitution, a material should have high mechanical strength and good biocompatibility  
 363 and bioactivity<sup>29</sup>. Titanium and its alloys used to manufacture implants and have a wide application. However,  
 364 from a biological standpoint, this type of material is relatively bioinert. A promising research line in the  
 365 development materials is creating bioactive coatings capable of enhancing the tissue regeneration responses  
 366 [3]. Sol-gels have been already used as coatings for Ti surfaces as they can release ions and other molecules  
 367 in a controlled manner<sup>24,30,31</sup>. Magnesium is an important ion involved in a wide range of biological functions;  
 368 it has been attracting increasing interest because of its potential applications in the biomedical field. The aim  
 369 of this study was to develop a new sol-gel coating acting as a release vehicle of Mg, to enhance bioactivity of  
 370 Ti materials and analyze the potential of this cation in bone regeneration.

371 The <sup>29</sup>Si-solid NMR showed that the incorporation of MgCl<sub>2</sub> into the sol-gel network did not affect the final  
 372 silica network crosslinking. In addition, Mg ions did not form crystalline structures (as MgCl<sub>2</sub> precipitates),  
 373 being were likely trapped on the hybrid structure through hydrogen bonding, Van der Waals or electrostatic

374 forces. Even though the Mg-doping did not change the material roughness, the contact angle significantly  
375 increased in comparison with the non-Mg coating regardless of the Mg concentration. Given that the  
376 roughness does not vary between compositions and that the degree of condensation of the synthesized  
377 networks is similar according to the chemical characterization, a possible explanation for the reduction  
378 observed in hydrophilicity could be associated with the presence of ions in the sol-gel structure and their  
379 effect in the Van der Waals and electrostatic forces<sup>32</sup>. As expected<sup>20,24</sup>, the rate of hydrolytic degradation  
380 increased as more MgCl<sub>2</sub> was incorporated into the sol-gel network, and more Mg<sup>2+</sup> was liberated. The release  
381 of this ion was stable until the end of the assay, reaching the values of 3 ppm in the material with the highest  
382 concentration of Mg (MT1.5Mg). None of the materials was cytotoxic to the MC3T3-E1 cells. Similarly,  
383 Romero-Gavilán *et al.*<sup>33</sup> and Martínez-Ibañez *et al.*<sup>17</sup> developed sol-gel coatings using MTMOS, TEOS and 3-  
384 glycidoxypropyltrimethoxysilane (GPTMS) that showed good bioactivity and biocompatibility. Yoshizawa *et al.*  
385<sup>34</sup> have reported that the Mg ion is non-cytotoxic at concentrations as high as 10 mM, thus confirming that  
386 the levels of Mg in the sol-gel coatings studied here were within the safe range.

387 Osteoblast cell adhesion and growth are promoted by Mg as it interacts with integrins, well-known  
388 transmembrane receptors necessary for cell adhesion and stability<sup>12</sup>. Yan *et al.*<sup>3</sup> have shown that bone-  
389 marrow-derived stem cells (BMSCs) seeded onto the titania nanotube arrays containing Mg develop extended  
390 filopodia and thicker cell walls, thus benefiting cell adhesion. Similarly, the MT1Mg and MT1.5Mg sol-gel  
391 coatings led to wide-spreading MC3T3-E1 osteoblastic cells, with protruding lamellipodia and a significantly  
392 higher surface area compared to the cells cultured in the MT. Zreiqat *et al.*<sup>8</sup> have shown that Mg ions added  
393 to a bioceramic substrate increase the cell adhesion and the expression of β1-, α5β1- and α3β1-integrins in  
394 human bone-derived cells (HBDC). Likewise, we showed that the Mg-doped coatings increase the expression  
395 of the β1- and α5-integrin genes, depending on the cation concentration and exposure time, thus confirming  
396 the effects of the coatings on cell adhesion.

397 Cell differentiation is critical for new bone formation<sup>35</sup>, and Mg-based biomaterials have proven effects on  
398 osteogenesis. Yan *et al.* [3] and Yoshizawa *et al.*<sup>34</sup> have shown that Mg-treated materials promote osteogenic  
399 differentiation in BMSCs. Gao *et al.*<sup>35</sup> have demonstrated an increase in ALP activity and osteogenic gene  
400 expression in MC3T3-E1 cells exposed to Mg-coated Ti6Al4V. Li *et al.*<sup>36</sup> evaluated the osteogenic properties  
401 of a nanoporous titanium coating with different concentrations of magnesium acetate, which was able to  
402 promote the adhesion, proliferation, and differentiation of bone marrow mesenchymal stem cells (BMSCs).  
403 Similarly, our Mg-doped sol-gel coatings increase the ALP activity on MT1.5Mg and TGF-β, OSX, and RUNX2  
404 gene expression, thus indicating an augmented osteoblastic cell differentiation and proliferation, which are  
405 indicators of bone formation<sup>37,38</sup>.

406 Chronic inflammation caused by implanted materials is associated with macrophages, which are the key  
407 players in the immune system<sup>39</sup>. They can assume two phenotypes: M1 and M2. The M1 macrophages are

408 involved in pro-inflammatory functions and the production of IL-1 $\beta$ , IL-12, and TNF- $\alpha$ . The M2 macrophages  
409 promote tissue healing and the production of IL-10 and TGF- $\beta$  <sup>40</sup>. There are several reports of magnesium  
410 effect on inflammation <sup>6,41</sup> and the response to biomaterials <sup>7,42–44</sup> by the regulation of macrophage  
411 polarization <sup>7</sup>. In this study, culturing the cells on the Mg-doped sol-gel materials caused a significant decrease  
412 in TNF- $\alpha$  secretion. It also significantly promoted the expression of IL-4 and TGF- $\beta$  genes and the secretion of  
413 TGF- $\beta$  in MT1.5Mg. These results suggest that the Mg-doped materials modulate the macrophage polarization  
414 towards the M2 phenotype. Li *et al.* <sup>7</sup> have reported similar results in RAW 264.7 cells exposed to Mg-doped  
415 titanium. They have verified that these materials cause a significant decrease in the levels of pro-inflammatory  
416 markers (CCR7, TNF- $\alpha$ , IL-1 $\beta$ ) and increase the abundance of anti-inflammatory markers (CD206, IL-4, IL-10).

417 The proteins from biological fluids spontaneously adsorbing onto the biomaterial surfaces play a major role in  
418 determining the interactions between implants and tissues. Understanding this phenomenon is essential to  
419 comprehend the cell responses and improve the design of biocompatible materials <sup>13</sup>. Here, the nLC-MS/MS  
420 analysis of the protein layer identified 22 proteins preferentially adsorbed onto the sol-gel coatings with Mg.  
421 Three proteins related to the complement system (CO9, C1QC, and CO3) and one associated with  
422 innate/adaptive immunological responses (SAMP) [43] were detected on these coatings. The complement  
423 system uses a large number of proteins that can induce an inflammatory response and opsonize pathogens  
424 [46]. However, this immunological response is controlled by numerous factors, which affect this cascade at its  
425 different stages. Among these are the plasma protease C1 inhibitor (IC1), vitronectin (VTNC), clusterin (CLUS)  
426 and complement factor H (CFAH) <sup>45</sup>. These four proteins were significantly more adsorbed onto the surfaces  
427 with Mg. The CLUS protein (8-fold increase in adsorption) prevents excessive inflammation through the  
428 regulation of complement activity and NF- $\kappa$ B pathway and reduces the apoptosis and oxidative stress <sup>46,47</sup>.  
429 IC1, a member of the serpin family of protease inhibitors, exerts an anti-inflammatory effect by regulating the  
430 complement system and interacting with extracellular matrices and cells <sup>48</sup>. Similarly, VTNC can moderate the  
431 intensity and duration of the inflammatory response to injury <sup>49</sup>. The CFAH protein is a critical regulator of the  
432 alternative complement pathway and has been directly associated with the maintenance of bone architecture.  
433 The balance in the interactions between osteoblasts and osteoclasts can be altered in the absence of CFAH,  
434 leading to a reduction in tissue quality <sup>50</sup>. Moreover, four apolipoproteins (APO2, APOA1, APOA4, and APOL1),  
435 known for their role in the metabolism of lipids and the inhibition of the complement system <sup>51</sup>, were also  
436 preferentially adsorbed onto Mg-containing surfaces. The increased affinity of Mg-doped coatings to these  
437 immune-response regulatory proteins can explain the anti-inflammatory potential observed *in vitro*.

438 The interaction of the host tissue cells with the implant surface is the key process in the integration of  
439 implanted material, modulating tissue regeneration. Several proteins related to cell adhesion and tissue  
440 regeneration preferentially adhered to the Mg-doped coatings. This is consistent with the *in vitro* results,  
441 which showed an increase in the osteogenic potential and cell adhesion on these materials. Desmoglein-1

442 (DSG1) and desmoplakin (DESP), mediators of cell–cell adhesion, are transmembrane glycoprotein  
443 components of desmosomes<sup>52</sup> and preferentially adhere to the Mg-enriched coatings. Moreover, VTCN, also  
444 found on the Mg-doped coatings, is one of the many proteins that regulate cell adhesion and tissue  
445 remodeling through the interaction with integrins<sup>53,54</sup>. Rivera-Chacon *et al.*<sup>55</sup> have shown that the  
446 nanoporous TiO<sub>2</sub> templates that absorbed more VTNC boosted the osteoblast attachment and proliferation  
447 and, consequently, improve osteoconduction. Li *et al.*<sup>56</sup> have reported that the VTNC adsorption onto a  
448 biomaterial surface affects the spreading of human mesenchymal stem cells (hMSCs) and integrin expression.  
449 The increase in cell adhesion observed on the Mg-doped coatings is likely to be a result of the augmented  
450 gene expression of the integrins regulated by Mg. However, the increased abundance of VTNC on such  
451 surfaces and its subsequent interactions with these transmembrane receptors might also contribute to the  
452 overall effect. The impact of Mg-based biomaterials on cell adhesion have been associated with the  
453 stimulation of integrins<sup>8</sup>. However, the role of proteins adsorbed onto the biomaterials, as far as we know,  
454 has never been considered. Further studies are needed to better understand the manner in which the  
455 adsorbed proteins, such as VTNC, might affect the interaction between Mg and integrins, and thus promote  
456 the cell adhesion.

457 Among the proteins associated with tissue regeneration, cystatin-A (CYTA), also known as stefin A, belongs to  
458 a family of cysteine protease inhibitors and is coded by the *CSTA* gene. One of the functions of this protein is  
459 the inhibition of cathepsin B (CATB), H, and L. These lysosomal cysteine proteinases that can modulate the  
460 architecture of the extracellular matrix<sup>57</sup>. They are associated with several inflammatory diseases, including  
461 periodontitis<sup>58–60</sup>. Moreover, the VTCN regulates cascades related to other biological processes, such as  
462 coagulation and fibrinolysis. This is achieved through its interaction with heparin and thrombin–antithrombin  
463 III complexes<sup>53</sup>. Another protein associated with coagulation, alpha-2-macroglobulin (A2MG), also  
464 preferentially adsorbs to the Mg-doped coatings. This protein is an antiprotease that functions as an inhibitor  
465 of plasmin, kallikrein, and thrombin<sup>61</sup> and has important functions in the clearance of active proteases. Such  
466 proteases are important agents in connective tissue diseases and well-known virulence factors<sup>62</sup>. The A2MG  
467 has been suggested as a marker for the blood compatibility with a biomaterial as it is a sensitive marker for  
468 plasma protease activation on artificial surfaces<sup>63</sup>.

469 These results show the potential of Mg in the development of biomaterials, revealing not only its overall effect  
470 on *in vitro* cell responses but also its role in the modulation of the protein adsorption patterns. It is possible  
471 to hypothesize that the well-known effects of magnesium biomaterials on cell adhesion, osteogenesis, and  
472 inflammation not only come from the properties of the ion itself, but also from the identified Mg-related  
473 proteins that attach to the surface upon implantation. With this, the results presented in this study shows a  
474 novel perspective of Mg in biomaterials as well as its effects on tissue regeneration.

475

## 476 5. Conclusion

477 The aim of this study was to further understand the effect of Mg on tissue regenerative processes. For that,  
478 we developed and characterized new Mg-enriched sol-gel coatings with a control release of the ion. The  
479 materials were successfully synthesized, with MgCl<sub>2</sub> well incorporated onto the sol-gel network, leading to a  
480 significant increase in the surface wettability in comparison with the base material. Unsurprisingly, the  
481 degradation increased with increasing Mg content, resulting in a steady release of Mg<sup>2+</sup> until the end of the  
482 assay. The Mg-doped coatings preferentially adsorbed proteins related to inflammatory responses, cell  
483 adhesion, tissue regeneration, and coagulation. Concerning the inflammatory response, the reduction in  
484 TNF- $\alpha$  secretion and the increase in TGF- $\beta$  and IL-4 gene expression indicate that the materials induced an  
485 anti-inflammatory phenotype. This was consistent with the increased adsorption of immune-system  
486 regulatory proteins (CLUS, CFAH, IC1 and VNTC). Moreover, the Mg-doped materials showed an increased  
487 affinity to the proteins related to cell adhesion (DESP, FILA2, and DSG1) and to the VTNC. This can explain the  
488 changes in the cell cytoskeleton arrangement with the consequent observed increase in the cell surface area.  
489 The Mg-doped materials also provoked an increase in the integrin gene expression (ITGA5 and ITGB1). In  
490 MC3T3-E1 osteoblastic cells, ALP activity was augmented in MT1.5Mg; this was accompanied by increased  
491 expression of TGF- $\beta$ , OSX and RUNX2 genes. This preferential adsorption of proteins related to tissue  
492 regeneration (CYTA and VTNC) indicated the regenerative potential of these materials. The anti-inflammatory  
493 properties of these materials in combination with improved cell adhesion and the observed osteogenic  
494 responses demonstrate their potential for enhanced bone healing, being this effect more prominent at the  
495 highest concentrations.

## 496 Author Contributions

497 **Andreia Cerqueira:** Conceptualization, Formal analysis, Investigation, Writing - Original Draft, Writing -  
498 Review & Editing **Francisco Romero-Gavilán:** Conceptualization, Formal analysis, Investigation, Writing –  
499 Original Draft, Writing - Review & Editing **Iñaki García-Arnáez:** Methodology, Investigation **Cristina Martínez-**  
500 **Ramos:** Methodology, Resources **Seda Ozturan:** Methodology, Resources **R. Izquierdo:** Resources, Funding  
501 acquisition **Mikel Azkargorta:** Investigation, Data Curation **Félix Elortza:** Data Curation, Writing - Review &  
502 Editing **Mariló Gurruchaga:** Conceptualization, Writing - Review & Editing, Funding acquisition **Isabel Goñi:**  
503 Conceptualization, Writing - Review & Editing, Funding acquisition **Julio Suay:** Conceptualization, Writing -  
504 Review & Editing, Funding acquisition

## 505 Conflicts of interest

506 No conflicts of interest are reported.

507

## 508 Acknowledgements

509 This work was supported by MINECO [MAT2017-86043-R; RTC-2017-6147-1], Generalitat Valenciana  
510 [GRISOLIAP/2018/091, APOSTD/2020/036, PROMETEO/2020/069], Universitat Jaume I under [UJI-B2017-37,  
511 Posdoc/2019/28], the University of the Basque Country under [GIU18/189] and Basque Government under  
512 [PRE\_2017\_2\_0044]. The authors would like to thank Raquel Oliver, Jose Ortega, José Miguel Pedra and Iraide  
513 Escobés for their valuable technical assistance and Antonio Coso (GMI-Ilerimplant) for producing the titanium  
514 discs.

## 515 References

- 516 1 E. O'Neill, G. Awale, L. Daneshmandi, O. Umerah and K. W. H. Lo, *Drug Discov. Today*, 2018,  
517 **23**, 879–890.
- 518 2 S. Castiglioni, A. Cazzaniga, W. Albisetti and J. Maier, *Nutrients*, 2013, **5**, 3022–3033.
- 519 3 Y. Yan, Y. Wei, R. Yang, L. Xia, C. Zhao, B. Gao, X. Zhang, J. Fu, Q. Wang and N. Xu, *Colloids*  
520 *Surfaces B Biointerfaces*, 2019, **179**, 309–316.
- 521 4 N. Nassif and I. Ghayad, *Adv. Mater. Sci. Eng.*, , DOI:10.1155/2013/532896.
- 522 5 M. M. Belluci, T. Schoenmaker, C. Rossa-Junior, S. R. Orrico, T. J. de Vries and V. Everts, *J.*  
523 *Nutr. Biochem.*, 2013, **24**, 1488–1498.
- 524 6 J. Sugimoto, A. M. Romani, A. M. Valentin-Torres, A. A. Luciano, C. M. Ramirez Kitchen, N.  
525 Funderburg, S. Mesiano and H. B. Bernstein, *J. Immunol.*, 2012, **188**, 6338–6346.
- 526 7 B. Li, H. Cao, Y. Zhao, M. Cheng, H. Qin, T. Cheng, Y. Hu, X. Zhang and X. Liu, *Sci. Rep.*, 2017,  
527 **7**, 42707.
- 528 8 H. Zreiqat, C. R. Howlett, a. Zannettino, P. Evans, G. Schulze-Tanzil, C. Knabe and M.  
529 Shakibaei, *J. Biomed. Mater. Res.*, 2002, **62**, 175–184.
- 530 9 H. Hornberger, S. Virtanen and A. R. Boccaccini, *Acta Biomater.*, 2012, **8**, 2442–2455.
- 531 10 M. Diba, F. Tapia, A. R. Boccaccini and L. a. Strobel, *Int. J. Appl. Glas. Sci.*, 2012, **3**, 221–253.
- 532 11 S. fang Zhao, Q. hong Jiang, S. Peel, X. xiang Wang and F. ming He, *Clin. Oral Implants Res.*,  
533 2013, **24**, 34–41.
- 534 12 Z. Wu, T. Tang, H. Guo, S. Tang, Y. Niu, J. Zhang, W. Zhang, R. Ma, J. Su, C. Liu and J. Wei,

- 535 *Colloids Surfaces B Biointerfaces*, 2014, **120**, 38–46.
- 536 13 S. Höhn, S. Virtanen and A. R. Boccaccini, *Appl. Surf. Sci.*, 2019, **464**, 212–219.
- 537 14 S. Galli, Y. Naito, J. Karlsson, W. He, I. Miyamoto, Y. Xue, M. Andersson, K. Mustafa, A.  
538 Wennerberg and R. Jimbo, *Acta Biomater.*, 2014, **10**, 5193–5201.
- 539 15 C. E. Wen, W. Xu, W. Y. Hu and P. D. Hodgson, *Acta Biomater.*, 2007, **3**, 403–410.
- 540 16 J. A. Oshiro, M. P. Abuçafy, E. B. Manaia, B. L. Da Silva, B. G. Chiari-Andréo and L. A.  
541 Chiavacci, *Polymers (Basel)*, , DOI:10.3390/polym8040091.
- 542 17 M. Martínez-Ibáñez, M. J. Juan-Díaz, I. Lara-Saez, A. Coso, J. Franco, M. Gurruchaga, J. Suay  
543 Antón and I. Goñi, *J. Mater. Sci. Mater. Med.*, , DOI:10.1007/s10856-016-5690-9.
- 544 18 N. Araújo-Gomes, F. Romero-Gavilán, I. García-Arnáez, C. Martínez-Ramos, A. M. Sánchez-  
545 Pérez, M. Azkargorta, F. Elortza, J. J. M. de Llano, M. Gurruchaga, I. Goñi and J. Suay, *J. Biol.*  
546 *Inorg. Chem.*, 2018, **23**, 459–470.
- 547 19 S. Oughlis, S. Lessim, S. Changotade, F. Bollotte, F. Poirier, G. Helary, J. J. Lataillade, V.  
548 Migonney and D. Lutomski, *J. Chromatogr. B Anal. Technol. Biomed. Life Sci.*, 2011, **879**,  
549 3681–3687.
- 550 20 F. Romero-Gavilán, N. Araújo-Gomes, A. Cerqueira, I. García-Arnáez, C. Martínez-Ramos, M.  
551 Azkargorta, I. Iloro, M. Gurruchaga, J. Suay and I. Goñi, *JBIC J. Biol. Inorg. Chem.*, 2019, **24**,  
552 563–574.
- 553 21 F. Romero-Gavilán, S. Barros-Silva, J. García-Cañadas, B. Palla, R. Izquierdo, M. Gurruchaga,  
554 I. Goñi and J. Suay, *J. Non. Cryst. Solids*, 2016, **453**, 66–73.
- 555 22 International Organization for Standardization, 2009, **3 ED**, 42.
- 556 23 International Organization for Standardization, .
- 557 24 A. Cerqueira, F. Romero-Gavilán, N. Araújo-Gomes, I. García-Arnáez, C. Martinez-Ramos, S.  
558 Ozturan, M. Azkargorta, F. Elortza, M. Gurruchaga, J. Suay and I. Goñi, *Mater. Sci. Eng. C*,  
559 2020, **116**, 111262.
- 560 25 F. Romero-Gavilán, A. M. Sanchez-Pérez, N. Araújo-Gomes, M. Azkargorta, I. Iloro, F.  
561 Elortza, M. Gurruchaga, I. Goñi and J. Suay, *Biofouling*, 2017, **33**, 676–689.

- 562 26 F. Romero-Gavilán, J. Carlos-Almeida, A. Cerqueira, M. Gurruchaga, I. Goñi, I. M. Miranda-  
563 Salvado, M. H. Vaz Fernandes and J. Suay, *Prog. Org. Coatings*, 2020, **147**, 105770.
- 564 27 H. N. Kim and S. K. Lee, *Geochim. Cosmochim. Acta*, 2013, **120**, 39–64.
- 565 28 G. Chernev, N. Rangelova, P. Djambazki, S. Nenkova, I. Salvado, M. Fernandes, A. Wu and L.  
566 Kabaivanova, *J. Sol-Gel Sci. Technol.*, 2011, **58**, 619–624.
- 567 29 C. Gao, S. Peng, P. Feng and C. Shuai, *Bone Res.*, 2017, **5**, 1–33.
- 568 30 F. Romero Gavilán, N. Araújo-Gomes, A. Cerqueira, I. Garcia Arnáez, C. Martínez Ramos, M.  
569 Azkargorta, I. Iloro, F. Elortza, M. Gurruchaga, J. Suay and I. Goñi, *JBIC J. Biol. Inorg. Chem.*,  
570 2019, **24**, 563–574.
- 571 31 F. Romero-Gavilán, N. Araújo-Gomes, I. García-Arnáez, C. Martínez-Ramos, F. Elortza, M.  
572 Azkargorta, I. Iloro, M. Gurruchaga, J. Suay and I. Goñi, *Colloids Surfaces B Biointerfaces*,  
573 2019, **174**, 9–16.
- 574 32 N. Novin, A. Shameli, E. Balali and S. Zomorodbakhsh, *J. Nanostructure Chem.*, 2020, **10**,  
575 69–74.
- 576 33 F. Romero-Gavilan, N. Araújo-Gomes, A. M. Sánchez-Pérez, I. García-Arnáez, F. Elortza, M.  
577 Azkargorta, J. J. M. de Llano, C. Carda, M. Gurruchaga, J. Suay and I. Goñi, *Colloids Surfaces*  
578 *B Biointerfaces*, 2017, **162**, 316–325.
- 579 34 S. Yoshizawa, A. Brown, A. Barchowsk and C. Sfei, *Acta Biomater.*, 2014, **10**, 2834–2842.
- 580 35 P. Gao, B. Fan, X. Yu, W. Liu, J. Wu, L. Shi, D. Yang, L. Tan, P. Wan, Y. Hao, S. Li, W. Hou, K.  
581 Yang, X. Li and Z. Guo, *Bioact. Mater.*, 2020, **5**, 680–693.
- 582 36 X. Li, M. Wang, W. Zhang, Y. Bai, Y. Liu, J. Meng and L. Zhang, *Int. J. Nanomedicine*, 2020,  
583 **15**, 6593–6603.
- 584 37 K. Janssens, P. Ten Dijke, S. Janssens and W. Van Hul, *Endocr. Rev.*, 2005, **26**, 743–774.
- 585 38 S. Wang, C. Xu, S. Yu, X. Wu, Z. Jie and H. Dai, *J. Mech. Behav. Biomed. Mater.*, 2019, **94**,  
586 42–50.
- 587 39 R. M. Lozano, B. T. Pérez-Maceda, M. Carboneras, E. Onofre-Bustamante, M. C. García-  
588 Alonso and M. L. Escudero, *J. Biomed. Mater. Res. Part A*, 2013, **101**, 2753–2762.



- 589 40 Q. Gu, H. Yang and Q. Shi, *J. Orthop. Transl.*, 2017, **10**, 86–93.
- 590 41 A. Mazur, J. A. M. Maier, E. Rock, E. Gueux, W. Nowacki and Y. Rayssiguier, *Arch. Biochem.*  
591 *Biophys.*, 2007, **458**, 48–56.
- 592 42 S. C. Cifuentes, F. Bensiamar, A. M. Gallardo-Moreno, T. A. Osswald, J. L. González-Carrasco,  
593 R. Benavente, M. L. González-Martín, E. García-Rey, N. Vilaboa and L. Saldaña, *J. Biomed.*  
594 *Mater. Res. Part A*, 2016, **104**, 866–878.
- 595 43 Q. Peng, K. Li, Z. Han, E. Wang, Z. Xu, R. Liu and Y. Tian, *J. Biomed. Mater. Res. Part A*, 2013,  
596 **101A**, 1898–1906.
- 597 44 M. D. Costantino, A. Schuster, H. Helmholz, A. Meyer-Rachner, R. Willumeit-Römer and B. J.  
598 C. Luthringer-Feyerabend, *Acta Biomater.*, 2020, **101**, 598–608.
- 599 45 N. S. Merle, S. E. Church, V. Fremeaux-Bacchi and L. T. Roumenina, *Front. Immunol.*, 2015,  
600 **6**, 1–30.
- 601 46 Z. C. Wu, J. T. Yu, Y. Li and L. Tan, in *Advances in Clinical Chemistry*, Academic Press Inc.,  
602 2012, vol. 56, pp. 155–173.
- 603 47 G. Falgarone and G. Chiocchia, *Adv. Cancer Res.*, 2009, **104**, 139–170.
- 604 48 A. E. Davis, P. Mejia and F. Lu, *Mol. Immunol.*, 2008, **45**, 4057–4063.
- 605 49 D. I. Leavesley, A. S. Kashyap, T. Croll, M. Sivaramakrishnan, A. Shokoohmand, B. G. Hollier  
606 and Z. Upton, *IUBMB Life*, 2013, **65**, 807–818.
- 607 50 J. J. Alexander, J. S. Sankaran, K. L. Seldeen, R. Thiyagarajan, A. Jacob, R. J. Quigg, B. R.  
608 Troen and S. Judex, *Immunobiology*, 2018, **223**, 761–771.
- 609 51 N. H. Cho and S. Y. Seong, *Immunology*, 2009, **128**, 479–486.
- 610 52 J. L. Johnson, N. A. Najor and K. J. Green, *Cold Spring Harb. Perspect. Med.*, ,  
611 DOI:10.1101/cshperspect.a015297.
- 612 53 S. Bierbaum, V. Hintze and D. Scharnweber, in *Comprehensive Biomaterials II*, Elsevier,  
613 2017, pp. 147–178.
- 614 54 T. J. Rowland, L. M. Miller, A. J. Blaschke, E. L. Doss, A. J. Bonham, S. T. Hikita, L. V. Johnson  
615 and D. O. Clegg, *Stem Cells Dev.*, 2010, **19**, 1231–1240.

616 55 D. M. Rivera-Chacon, M. Alvarado-Velez, C. Y. Acevedo-Morantes, S. P. Singh, E. Gultepe, D.  
617 Nagesha, S. Sridhar and J. E. Ramirez-Vick, *J. Biomed. Nanotechnol.*, ,  
618 DOI:10.1166/jbn.2013.1601.

619 56 T. Li, L. Hao, J. Li, C. Du and Y. Wang, *Bioact. Mater.*, 2020, **5**, 1044–1052.

620 57 S. M. Soond, M. V. Kozhevnikova, A. A. Zamyatnin and P. A. Townsend, *Pharmaceuticals*,  
621 2019, **12**.

622 58 X. Li, Z. Wu, J. Ni, Y. Liu, J. Meng, W. Yu, H. Nakanishi and Y. Zhou, *Oxid. Med. Cell. Longev.*, ,  
623 DOI:10.1155/2016/7894247.

624 59 E. Ichimaru, M. Tanoue, M. Tani, Y. Tani, T. Kaneko, Y. Iwasaki, K. Kunimatsu and I. Kato,  
625 *Inflamm. Res.*, 1996, **45**, 277–282.

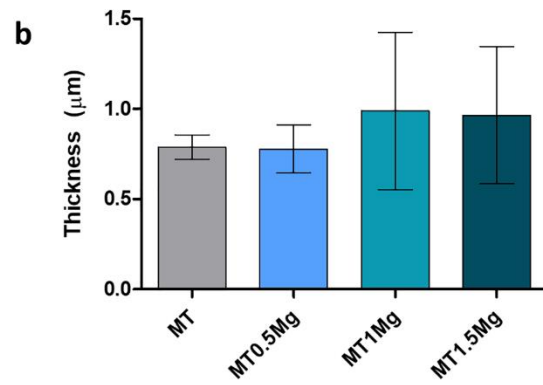
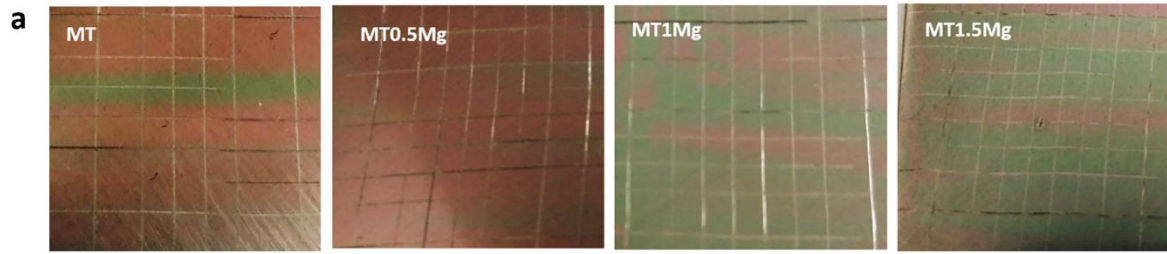
626 60 K. Kunimatsu, K. Yamamoto, E. Ichimaru, Y. Kato and I. Kato, *J. Periodontal Res.*, 1990, **25**,  
627 69–73.

628 61 J. H. Cater, M. R. Wilson and A. R. Wyatt, *Oxid. Med. Cell. Longev.*, 2019, **2019**, 9.

629 62 P. B. Armstrong and J. P. Quigley, *Dev. Comp. Immunol.*, 1999, **23**, 375–390.

630 63 D. Biloft, J. B. Gram, A. Larsen, A. M. B. Münster, J. J. Sidemann, K. Skjoedt and Y.  
631 Palarasah, *Clin. Biochem.*, 2017, **50**, 1203–1208.

632



633

634 **Supplementary Figure 1.** Cross-cut test results (a) and thickness measurements (b). Results are  
635 shown as means  $\pm$  SE.

636